ELSEVIER

Engineering Analysis with Boundary Elements 25 (2001) 467–473

ENGINEERING ANALYSIS *with* BOUNDARY ELEMENTS

www.elsevier.com/locate/enganabound

Technical Note

Boundary element analysis of fatigue crack propagation micromechanisms in austempered ductile iron

J. Ortiz[1], A.P. Cisilino*, J.L. Otegui

Welding and Fracture Division — INTEMA, Faculty of Engineering, Universidad Nacional de Mar del Plata — CONICET, Av. Juan B. Justo 4302 (7600) Mar del Plata, Argentina

Received 26 May 2000; revised 20 June 2000; accepted 4 December 2000

Abstract

The Dual Boundary Element Method (DBEM) is used in this work to model the micro mechanics of fatigue crack propagation in austempered ductile iron (ADI). Emphasis is put in devising accurate procedures for the evaluation of the interaction effects between very close crack–microcrack arrays. Fracture parameters are computed via the so-called one-point displacement formula using special crack-tip elements. Crack propagation is modelled using an incremental crack extension analysis; with crack extensions calculated using a propagation law that accounts for the near-threshold regime. Obtained results are in agreement with experimental observations, providing evidence to fracture mechanics models proposed in the literature. © 2001 Elsevier Science Ltd. All rights reserved.

Keywords: Austempered ductile iron; Fatigue crack propagation; Graphite

1. Introduction

Cast irons are two-phase metallic composites in which cementite or graphite particles are arranged in an iron-based matrix. Both, matrix microstructure and particle shape and type depend on chemical composition and thermal treatment. Austempered ductile iron (ADI) is the result of special heat treatments of a conventional nodular cast iron with selectively added alloying elements. ADI combines good elongation and toughness with high tensile strength; combination that increases the resistance to wear and fatigue when compared to other ductile irons. The material has a wide range of industrial applications, as is the case of chain wheels, lines of cement mills, railroad wheels, gears and automotive crankshafts. The application of ADI will continue to grow as the design engineer familiarizes with their properties [1].

Greno et al. [2] carried out a quantitative study of the morphology of fatigue crack propagation in ADI, showing that the crack path preferentially intersects graphite nodules. They also observed that a microcracking process takes place in the region of high stress concentration around the tip of macroscopic cracks. These microcracks emanate from irregularities and sharp corners located on the nodule-matrix interfaces, as shown in Fig. 1. The occurrence of subcritical multiple microcrack initiation at graphite nodules has been reported by other authors even at stress levels close to the fatigue endurance limit [3]. Greno et al. [2] propose that as microcracks simultaneously propagate besides the main crack, the available elastic energy for the propagation of the main crack is diminished mainly because of the creation of a larger crack surface. In addition there is growing evidence of the shielding effect that microcracking has on the tip of a dominant macrocrack, redistributing and reducing the average near-tip stresses [4]. Sources of stress redistribution are the reduction of elastic moduli resulting from microcracking and inelastic strains arising from the release of residual or transformation stresses when microcracks are formed. All the above-mentioned mechanisms provide evidence to explain the relatively low propagation rates and high effective propagation threshold values of ADI when compared with those of steels. For these mechanisms to operate it is essential that microcracks arrest and be highly stable in the arrest configuration [4].

A two-dimensional numerical study of the micromechanics of fatigue crack propagation in ADI is presented in this paper in order to provide further evidence to validate the fracture mechanics models mentioned above. The numerical tool for the analysis is based on the Dual Boundary Element Method (DBEM), customized for the

* Corresponding author. Tel.: +54-223-4816600; fax: +54-223-4810046.

E-mail address: cisilino@fi.mdp.edu.ar (A.P. Cisilino).

[1] On leave from Universidad Privada del Norte, Trujillo, Peru.

PII: S0955-7997(01)00034-0

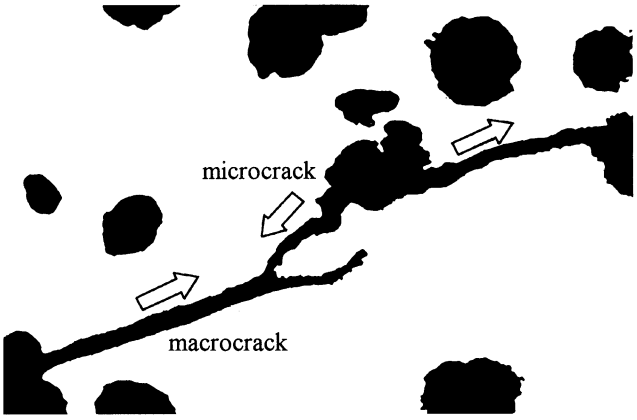

Fig. 1. Enlarged × 500 micrograph showing the fatigue crack propagation mechanism in ADI [2]. Note sharp edges in 'spheroidal' nodules (White: matrix, black: graphite nodules).

accurate evaluation of the interaction effects between cracks, microcracks and graphite nodules.

2. Method of analysis

2.1. BEM formulation

Numerical modelling of fatigue crack propagation requires the capability of predicting the direction and amount of crack growth for each given load increment, as well as the robustness to update the numerical model to account for the changing crack geometry. The DBEM is a well-established numerical technique in this area of fracture mechanics as it eliminates the remeshing problems, which are typical of domain methods and other boundary element formulations [5]. General mixed-mode crack problems can be solved with the DBEM in a single region formulation, where the displacement boundary integral equation is applied on one of the crack surfaces and the traction boundary integral equation on the other. Crack growth process is efficiently simulated with an incremental analysis, where crack extensions are modelled by adding new discontinuous elements ahead the crack tips. This simple strategy is robust and allows the DBEM to effectively model general edge or embedded crack problems; crack tips, crack-edge corners and crack kinks do not require special treatment, since they are not located at nodal points where collocation is carried out. For further details on the DBEM formulation and implementation the reader is referred to the works by Portela et al. [6,7].

2.2. Evaluation of crack-tip stress intensity factors

Accurate evaluation of crack tip stress intensity factors K is of main importance for the effective analysis of crack propagation problems. In particular for the kind of problem tackled in this work, where propagation of close crack–microcrack arrays is analysed, precise assessment of interaction effects constitutes a key factor. In this sense, three different techniques were considered for the evaluation of K: the J-integral [8], the Energy Domain Integral (EDI) [9] and the so-called one point displacement formula [8]. DBEM implementation of the J-integral is due to Portela et al. [7], while implementation of the EDI follows the one proposed by Cisilino et al. [10]. Stress intensity factors through the one-point displacement formula are simply obtained by replacing crack face displacements in the expressions of the near crack-tip displacement fields. On the other hand, its efficiency strongly depends on the accuracy of the displacements calculated on the crack surfaces.

In order to have a better representation of the crack-tip region, special crack-tip elements which exhibit the correct $\sqrt{r}$ variation for the displacement field were implemented. The approach devised by Yamada et al. [11] for finite elements was employed to derive the special shape functions for the displacement fields in discontinuous elements. The performance of special elements for crack–microcrack problems was assessed by comparison with results due to Rubinstein [12], who provided an analytical solution for K at the crack tip of a semi-infinite crack interacting with a collinear microcrack in an infinite sheet (see Fig. 2). BEM models where constructed following the criteria of Dutta et al. [13], who suggest that for a crack length a at least twenty times larger than the length of the microcrack $2c$, interaction behaviour can be assimilated to that of a semi-infinite crack. Differences between computed and reference K values for crack tip A are shown in Fig. 2, for a wide range of relative microcrack positions h/c. Results are presented as functions of normalized crack-tip element length L/a. It can be observed that differences less than 2% are obtained with crack-tip elements of length $L/a < 0.01$. For all cases best results were obtained when displacements of the node closest to the crack tip were considered for K computations.

Performance of the J-integral and the EDI for very small integration paths was also tested. Computed results for the

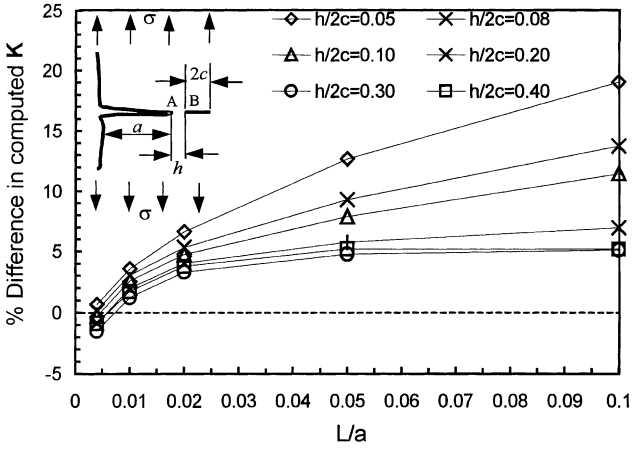

Fig. 2. Difference (Percentage) of computed K values with respect to Rubinstein's solution for crack tip A [12].

Table 1
Comparison of K results for a semi-infinite crack interacting with a collinear microcrack in an infinite sheet

h/c	$K_A/F\sigma\sqrt{\pi a}$				$K_B/\sigma\sqrt{\pi c}$		
	Displ. form	J integral	EDI	Ref. [11]	Displ. form	J integral	EDI
0.05	1.74	1.82	1.83	1.75	27.37	28.98	29.16
0.08	1.55	1.59	1.60	1.55	23.08	23.79	23.97
0.1	1.47	1.50	1.51	1.47	21.11	21.65	21.83
0.2	1.29	1.29	1.30	1.28	16.10	16.28	16.28
0.3	1.22	1.21	1.22	1.20	13.60	13.60	13.60
0.4	1.18	1.16	1.17	1.17	11.99	11.99	12.16

macrocrack tip A and the microcrack tip B (see Fig. 2) using both techniques are presented in Table 1, together with the results obtained with the displacement formula and reference values. Lengths of the special crack-tip element correspond to $L/a = 0.005$ and $L/c = 0.05$ for the crack and microcrack, respectively. Integration paths and domains were chosen circular, with a radius equal to the distance from the crack tip to the closest node on the crack surface. Data in the table show that for distances $h/c > 0.1$, results obtained using the three techniques are almost identical. On the other hand, for $h/c < 0.1$, results obtained using the J-integral and the EDI tend to be larger than those of the displacement formula. In the case of tip A, for which the analytical solution exists, the displacement formula is the most accurate with results differing less than 1% from those in the reference. Reference results for the microcrack tip B are not available. The effect of the special element length was found not to be as marked as for tip A. For special elements with lengths $L/c < 0.05$ the variations in the results was less than 1%. Although the three techniques perform similarly the one-point displacement formula was preferred for the rest of this work, as the definition of appropriate integration paths or domains for general crack–microcrack arrays could be sometimes difficult.

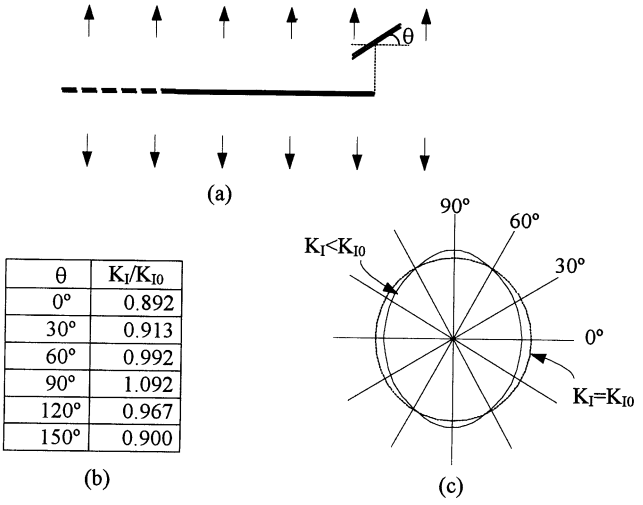

θ	K_I/K_{I0}
0°	0.892
30°	0.913
60°	0.992
90°	1.092
120°	0.967
150°	0.900

Fig. 3. Crack–microcrack interaction: (a) problem geometry, (b) computed results, (c) variation of the SIF at the main crack tip as function of the microcrack orientation (from Kachanov et al. [14]).

A more general test problem for which the microcrack is not collinear with the main crack is shown in Fig. 3. Kachanov et al. [14] showed that interaction effects for this case could either increase or decrease K at the tip of the main crack, depending on the microcrack orientation angle θ. Only a qualitative comparison between results is shown in for this case, as numerical values are not given in the reference. Results show an excellent correlation.

2.3. Crack extension analysis

The incremental crack-extension analysis assumes a piece-wise linear discretization of the unknown crack path. For each increment of the crack extension, the DBEM is applied to carry out a stress analysis and crack tip stress intensity factor computation. Magnitude and direction of crack increments are then computed for each crack, and the crack extended accordingly by adding new elements ahead of the previous crack tips. The above steps are repeated sequentially until a specified number of crack-extensions is reached.

The fatigue propagation formula due to Klesnil and Lukas [15] was chosen to correlate the incremental size and the number of load cycles, as it accounts for the near-threshold regime

$$\frac{da}{dN} = C(\Delta K^m - \Delta K_{th}^m), \tag{1}$$

where da/dN is the rate of change in crack length per load cycle; C and m are material constants; ΔK_{th} accounts for the threshold value below which cracks do not propagate and ΔK is the cyclic value of equivalent stress intensity factor that accounts for the combined effects of mode I and II. Employing the expression proposed by Tanaka [16], the resultant expression for ΔK is

$$\Delta K^2 = \Delta K_I^2 + 2\Delta K_{II}^2. \tag{2}$$

The effect of closure on crack propagation rate is acquainted though the 'effective' crack tip stress intensity factor range

$$\Delta K_{eff} = K_{max} - K_{op}, \tag{3}$$

where K_{op} corresponds to the value of K at which the crack

tip opens. Closure data is usually presented in terms of Elber [17] closure ratio $U = \Delta K_{\text{eff}}/\Delta K$.

Finally, the magnitudes of crack-extensions are computed using Expressions (1) and (3) in an incremental form:

$$\Delta a = C[(U\Delta K)^m - \Delta K_{\text{th}}^m]\Delta N. \quad (4)$$

Among the several available criteria for computing the local direction of crack growth, the minimum strain energy criterion [18] is employed in this work. This is used in conjunction with the predictor–corrector algorithm due to Portela et al. [6] to ensure that a unique final crack path is achieved regardless of the crack-extension length. It is also worth to mention that as the model involves the propagation of multiple cracks, the computation of the crack extensions is based on a fixed value of load cycles for all cracks in order to allow them to extend differently.

3. Application to ADI

3.1. Fatigue crack propagation

Simple models consisting in a macrocrack and a microcracked nodule were considered first in order to study the effect of crack closure on the crack–microcrack interaction mechanism. Crack closure is a relevant factor when assessing the mechanism of fatigue crack propagation in ADI as it behaves differently for macrocracks and microcracks. In this sense is worth to note that while closure levels can be significant for macrocracks, microcracks are mostly closure free [19]. The model geometry and discretization, together with the resulting crack paths for three closure levels are shown in Fig. 4. As for all models presented in this work, graphite nodules were assimilated to circular voids. This assumption implies to consider a material with 100% nodularity, and to neglect the mechanical response of graphite when compared with that of the metal matrix. Metal matrix is assumed isotropic and linear elastic. Material constants for the propagation law were chosen according to experimental results as $C = 4.43 \times 10^{-10}$, $m = 2.85$, $\Delta K_{th} = 5\ MPa\sqrt{m}$. Closure levels were selected as $U = 1$ (no closure), $U = 0.6$ and $U = 0$, the last one corresponding to a limiting case for which the main crack does not propagate.

Fig. 5 illustrates the evolution of ΔK with load cycles N for the three closure levels. Stress intensity factor ranges ΔK are presented normalized with respect to ΔK_{th}, in such a way that ratios greater than one represent propagating cracks, while values below one stand for non-propagating cracks. Note that as the macrocrack approaches the microcrack emanating from the nodule, interaction effects cause a substantial increase in the ΔK at crack tip A, which propagates in opposite sense to the macrocrack growth direction until joining it. As soon as the macrocrack and the first microcrack coalesce, microcrack B on the opposite side of the nodule becomes dominant, taking the role as macrocrack tip. The effect of closure is of delaying the process as the macrocrack slows down its propagation rate, taking longer for it to coalesce with first microcrack.

A more general situation is shown in Fig. 6, where a macrocrack propagates now into an array of randomly distributed nodules with microcracks labelled from A to H. Obtained results allow extending the propagation mechanism of the previous example, as the tips B, D, F and H successively take the role of the macrocrack tip. At the same time, microcracks A, C, E and G propagate towards the macrocrack tip, to finally become dormant due to load shielding effects. Microcracks I, J, K and L do not take part in the main propagation path, however they present the same general behaviour of the other microcracks. In this case, more than one microcrack propagate simultaneously towards the tip of the dominant crack, justifying the presence of the crack 'bifurcations' observed during experiments [2].

3.2. Effect of nodule size and distribution

A major feature in the above analyses is that only a limited number of nodules were included in the models, while they are actually distributed over the entire domain. The effect of nodule size and distribution on the propagation mechanism is considered in this section through the analysis of the stress fields in the uncracked ADI microstructure. The ratio r/d, where r is the average nodule radius and d the

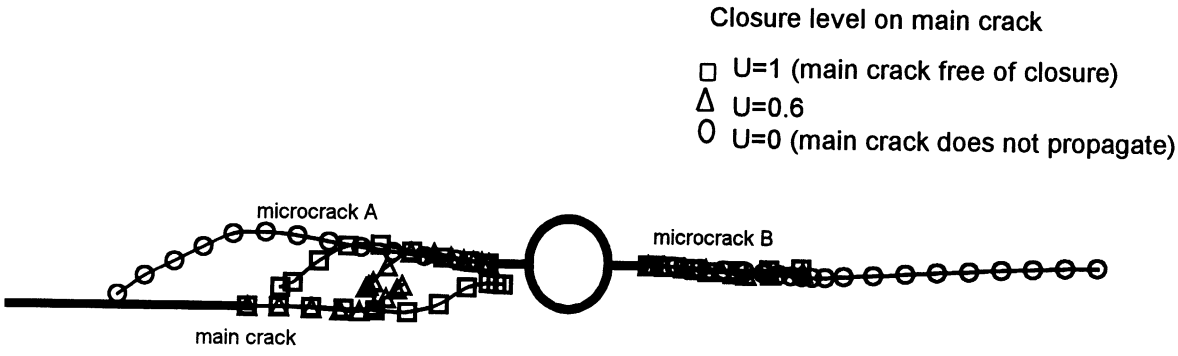

Fig. 4. Effect of closure level on crack–microcrack interaction mechanism.

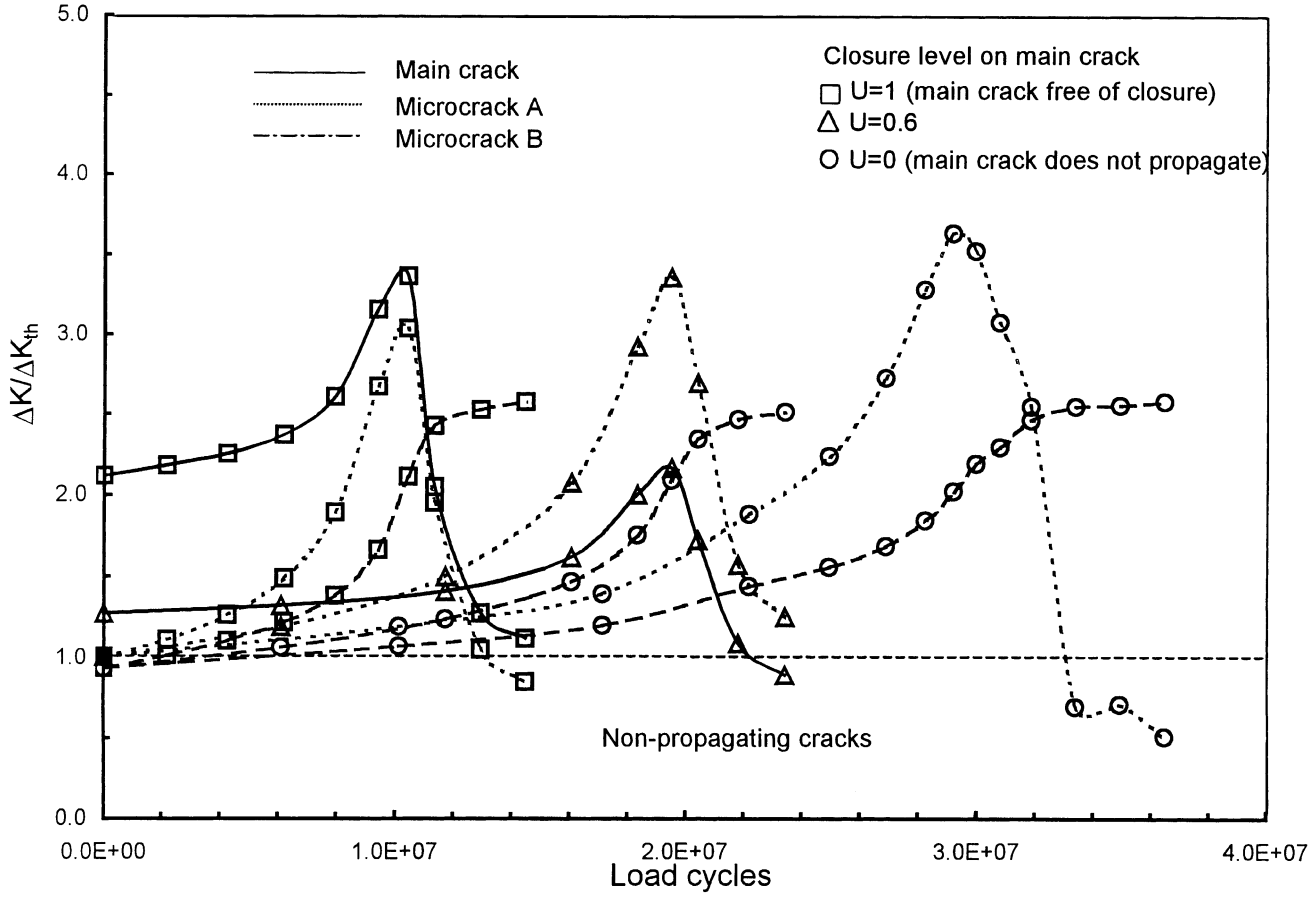

Fig. 5. Evolution of ΔK values with load cycles.

average minimum distance between nodule centres was chosen as the characteristic parameter (see Fig. 7(a)). Results of a statistical analysis of measurements performed on standard ADI micrographs using an image-processing software [20] showed that for a wide range of nodular counts, ranging from 60 to 600 nodules/mm^2, the average values of r/d as well as its standard deviation are almost constant. The referred value corresponds to $r/d = 0.25$ with a standard deviation of around 35%. In view of this results BEM models were carried out on a series of randomly generated ADI microstructures with r/d values ranging from 0.1 to 0.3. A typical model discretization is shown in Fig. 7(b), where schematics with the location of the internal-point arrays used for stress computations are also shown. Locations of the internal points were selected to evaluate the characteristics of the stress fields in the vicinity of nodules and along lines oriented perpendicularly to the applied load (A and B in Fig. 7(b)).

Statistical analysis of the model results used in conjunction with a weight-function analysis showed that [21]:

- Stress fields in the vicinity of nodules averages those corresponding to an isolated hole, with standard deviations increasing with r/d. Maximum principal stresses on nodule surfaces take place in the vicinity of the

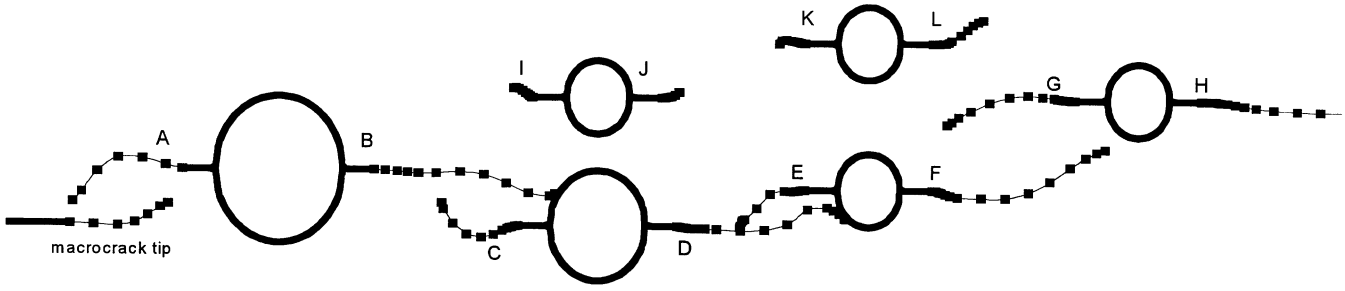

Fig. 6. Evolution of propagation paths for a general module array.

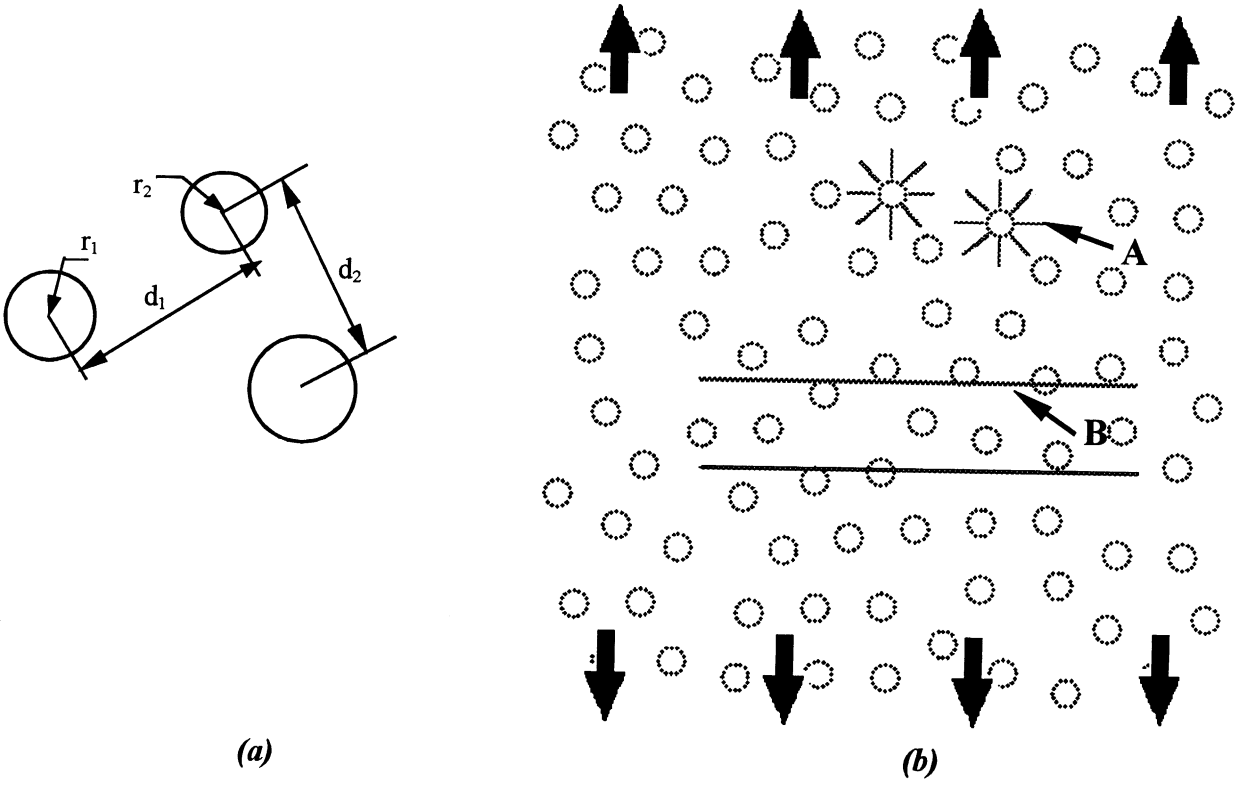

Fig. 7. BEM model of ADI microstructure: (a) characteristic dimensions of the problem; (b) locations of internal-point arrays.

nodule 'equators', converting these regions in preferential locations for the initiation of microcracks. A standard deviation of around 10% is expected for K values at the tip of microcracks emanating from nodules, provided the microcrack length is less than the average nodule radius ($c < r$). The deviation grows up to 20% for microcrack lengths $c = 2r$.

- There exists a clear periodicity in the maximum principal stresses along paths defined perpendicularly to the direction of the remote applied load. Analysis of the data using fast Fourier transformations allowed concluding that this period corresponds to half the minimum nodule distance $d/2$. This makes K levels for a single macrocrack in ADI lower than that of a macrocrack in a homogeneous material, but the difference strongly depends on the macrocrack length $2a$. In order to ensure a difference less than 10%, crack lengths $2a > 40d$ are necessary. Deviation can be reduced to 7% if crack lengths $2a > 100d$ are considered.

4. Discussion

Fracture mechanics models for the micromechanisms of fatigue crack propagation in ADI are based on the existence of microcracking at the tip of the dominant macrocrack. Propagation of these microcracks diminishes the available elastic energy for the propagation of the macrocrack because of the creation of a larger crack surface. In addition, microcracks have a shielding effect on the tip of a dominant macrocrack, redistributing and reducing the average near-tip stresses. For these mechanisms to operate it is essential that the microcracks arrest and be highly stable in the arrest configuration [4].

DBEM results from the previous section provide evidence to corroborate above models. It is shown that a macrocrack advances through a mechanism of interaction and coalescence of the microcracks that develop from nodules. The same time it is observed those microcracks that propagate beside the macrocrack but finally do not take part in the main propagation path become dormant and stable due to shielding effects. The estimates of the deviation ranges for ΔK due to the presence of nodules show the dependence of the propagation mechanism with the load level. For applied loads that induce ΔK levels close to ΔK_{th} on the macrocrack tip, deviation ranges can easily situate ΔK levels under propagation threshold inducing the mechanism to stop. On the other hand, as the difference between the applied ΔK levels and ΔK_{th} increases, the effect of deviation bounds in ΔK is less important. Although they could affect the general propagation rate, the probability of the mechanism to stop diminishes. This is verified in fractographic observations, which showed a decrement in the

frequency of appearance of crack bifurcations at low levels of applied ΔK [2].

Crack closure showed to be another important factor to be considered as it reduces the general rate of advance and may in some cases cause locally the premature arrest of crack growth. Many mechanisms have been identified for fatigue crack closure in ADI, such us plasticity, residual stresses, crack face and stress-induced metallurgical transformations. In this area, more observational data is needed in order to obtain accurate quantitative estimates of the closure effect.

At the same time, it is important not to forget the three-dimensional nature of the problem. Long and short cracks have different behaviour due to the relative size of their crack fronts. The presence of irregularities causes an effect more attenuated for a wide front than for a reduced one. Therefore, it can be said that the increment in the value of ΔK factor calculated for the main crack tip presents only a local effect that would be almost imperceptible if only the presence of a single nodule next to the crack front is considered. Propagation rate of the main crack corresponds to an average of all the phenomena that simultaneously take place along the whole extension of the crack front. In this sense, it is not expected for the obtained results to yield actual numbers for real cases, but to be in accordance with experimental observations allowing validating fracture mechanics models.

5. Conclusions

The DBEM was successfully employed in this work to study the micromechanism of fatigue crack propagation in ADI. The modelling tool was customized to tackle the fatigue propagation of very close crack-microcrack arrays. The one-point displacement formula was employed together with special crack-tip elements and a suitable discretization strategy for the evaluation of stress intensity factors. The procedure allowed for the accurate evaluation of the interaction effects between cracks and microcracks.

The devised methodology proved to be a potent tool to help understanding the propagation mechanisms. Obtained results are in agreement with experimental observations, and provide further evidence to validate theoretical fracture mechanics models to explain the relatively low propagation rates and high effective threshold values measured in this material.

Acknowledgements

This work was financed by grant PICT 12-04586 of Agencia Nacional de Promoción Científica de la República Argentina. Authors wish to thank CONICET and Organization of American States (OAS) for additional funding. Authors are also grateful to Professor M.H. Aliabadi for providing DBEM software.

References

[1] Ductile iron data for design engineers, QIT-Fer & Titane, 1990.
[2] Greno GL, Otegui JL, Boeri RE. Mechanisms of fatigue crack growth in austempered ductile iron. Int J Fract 1999;21:35–43.
[3] Marrow TJ. Short fatigue cracks in austempered ductile iron (ADI). Fatigue Fract Engng Mater Struct 2000;23:425–34.
[4] Hutchinson JW. Crack tip shielding by micro-cracking in brittle solids. Acta Metall 1987;35(7):1605–19.
[5] Aliabadi MH. Boundary element formulations in fracture mechanics. Appl Mech Rev 1997;50(2):83–96.
[6] Portela A, Aliabadi MH, Rooke DP. The dual boundary element method: effective implementation for crack problems. Int J Num Meth Engng 1992;33:1267–87.
[7] Portela A, Aliabadi MH, Rooke DP. Dual boundary element incremental analysis of crack propagation. Comput Struct 1993;46(2): 237–47.
[8] Aliabadi MH, Rooke DP. Numerical fracture mechanics. London: Kluwer Academic Publishers, 1994.
[9] Shih CF, Moran B, Nakamura T. Energy release rate along a three-dimensional crack front in a thermally stressed body. Int J Fract 1986;30:79–102.
[10] Cisilino AP, Aliabadi MH, Otegui JL. Energy domain integral applied to solve centre and double-edge crack problems in three dimensions. Theor Appl Fract Mech 1998;29:237–56.
[11] Yamada Y, Ezawa Y, Nishiguchi I. Reconsiderations on singularity or crack tip elements. Int J Num Meth Engng 1979;14:1525–44.
[12] Rubinstein AA. Macrocrack interaction with semi-infinite microcrack array. Int J Fract 1985;27:113–9.
[13] Dutta B, Maiti S, Kakodkar A. Analysis of crack–microcrack interactions and doubly kinked cracks using multiples singular point elements. Engng Fract Mech 1991;38/23:215–23.
[14] Kachanov M, Montagut E. Interaction of a crack with certain microcrack arrays. Engng Fract Mech 1986;25(5/6):625–36.
[15] Klesnil M, Lukas P. Influence of strength and stress history on growth and stabilisation of fatigue cracks. Engng Fract Mech 1972;4:77–92.
[16] Tanaka K. Fatigue crack propagation from a crack inclined to the cyclic tensile axis. Engng Fract Mech 1974;6:493–507.
[17] Elber W. The significance of fatigue crack closure damage tolerance in aircraft structures. ASTM STP 1971;486:230–47.
[18] Sih GC. Mechanics of fracture initiation and propagation. Dordrecht: Kluwer Academic Publishers, 1991.
[19] Leis BN, Hoper AT, Ahmad J. Critical review of the fatigue growth of short cracks. Engng Fract Mech 1986;23(25):883–98.
[20] Image-Pro Plus, Media Cybernetics Inc., USA.
[21] Ortiz JE, Desarrollo de una herramienta computacional para el modelado de propagación de fisuras múltiples por fatiga, Msc Thesis, Facultad de Ingeniería, Universidad Nacional de Mar del Plata, Argentina, 2000.